REGULAR ARTICLE

blood advances

Targeting CDC42 reduces skeletal degeneration after hematopoietic stem cell transplantation

Theresa Landspersky,[1] Merle Stein,[2] Mehmet Saçma,[3] Johanna Geuder,[4] Krischan Braitsch,[1] Jennifer Rivière,[1] Franziska Hettler,[1] Sandra Romero Marquez,[1] Baiba Vilne,[5] Erik Hameister,[1] Daniel Richter,[2] Emely Schönhals,[1] Jan Tuckermann,[2] Mareike Verbeek,[1] Peter Herhaus,[1] Judith S. Hecker,[1] Florian Bassermann,[1] Katharina S. Götze,[1] Wolfgang Enard,[4] Hartmut Geiger,[3] Robert A. J. Oostendorp,[1,*] and Christina Schreck[1,*]

[1]School of Medicine, Department of internal Medicine III, Technical University of Munich, Munich, Germany; [2]Institute of Comparative Molecular Endocrinology, and [3]Institute of Molecular Medicine, Stem Cells, and Aging, Ulm University, Ulm, Germany; [4]Anthropology and Human Genomics, Faculty of Biology, Ludwig-Maximilians University, Munich, Germany; and [5]Bioinformatics Laboratory, Rīga Stradiņš University, Riga, Lettland

Key Points

- CDC42 activity regulates F-actin fiber alignment, mitochondrial function, and mitophagy in MSPCs in a bone marrow transplant setting.
- Attenuation of CDC42 activity improves MSPC quality to increase both bone volume and trabecular bone thickness.

Osteopenia and osteoporosis are common long-term complications of the cytotoxic conditioning regimen for hematopoietic stem cell transplantation (HSCT). We examined mesenchymal stem and progenitor cells (MSPCs), which include skeletal progenitors, from mice undergoing HSCT. Such MSPCs showed reduced fibroblastic colony-forming units frequency, increased DNA damage, and enhanced occurrence of cellular senescence, whereas there was a reduced bone volume in animals that underwent HSCT. This reduced MSPC function correlated with elevated activation of the small Rho guanosine triphosphate hydrolase CDC42, disorganized F-actin distribution, mitochondrial abnormalities, and impaired mitophagy in MSPCs. Changes and defects similar to those in mice were also observed in MSPCs from humans undergoing HSCT. A pharmacological treatment that attenuated the elevated activation of CDC42 restored F-actin fiber alignment, mitochondrial function, and mitophagy in MSPCs in vitro. Finally, targeting CDC42 activity in vivo in animals undergoing transplants improved MSPC quality to increase both bone volume and trabecular bone thickness. Our study shows that attenuation of CDC42 activity is sufficient to attenuate reduced function of MSPCs in a BM transplant setting.

Introduction

Osteoporosis and osteopenia are clinically well-documented long-term complications after allogeneic hematopoietic stem cell transplantation (allo-HSCT).[1,2] Myeloablation through chemotherapeutic treatment or irradiation remains a crucial preconditioning regimen for successful donor stem cell engraftment and regeneration of hematopoiesis in allo-HSCT. Osteoporosis is found in approximately half of HSCT recipients even 10 years after allo-HSCT, regardless of the type of the prior preconditioning regimen.[3,4] In addition, there are signs of senile osteoporosis in allo-HSCT recipients, which are independent of the age of the patient who received transplantation.[5] The observed bone degeneration in such patients suggests that the function of osteoprogenitors in the bone marrow (BM) niche is inefficient and/or incomplete after allo-HSCT or that the rate of osteodestruction is increased.

Submitted 7 February 2024; accepted 16 June 2024; prepublished online on *Blood Advances* First Edition 19 August 2024. https://doi.org/10.1182/bloodadvances.2024012879.

*R.A.J.O. and C.S. are joint senior authors.

Data are available on request from the corresponding author, Christina Schreck (christina.schreck@tum.de).

The full-text version of this article contains a data supplement.

The hematopoietic BM niche is an ecosystem of many different cell types that respond to external triggers and strive to restore and maintain optimal conditions for both hematopoiesis and bone remodeling.[6] The consequences of cellular stress and aging in HSCs, have been explored in several studies.[6,7] The impact of stress responses and aging on the function of BM niche cell populations is still largely unclear.[8-10] In previous work we showed that intermittent exposure to the cytostatic agent 5-fluorouracil leads to *Wnt5a*-dependent F-actin misalignment in BM-derived mesenchymal stem and progenitor cells (MSPCs), which is associated with incorrect positioning of autophagosomes and lysosomes.[11] Diminished autophagy is 1 of the hallmarks of aging,[12] which can also be found in MSPCs from aging individuals.[13] Furthermore, reduced autophagy is associated with reduced expression of selective autophagy receptors, such as optineurin (OPTN), Tax1-binding protein 1, or sequestosome 1.[14] In MSPCs, such changes reduce osteogenesis and favor adipogenesis, which contributes to degenerative bone loss (osteoporosis) with increasing age.[15]

Here, we identify cellular and molecular changes in MSPCs from mice undergoing HSCT. Our analyses showed clear signs of MSPC dysfunction: oxidative stress, reduced autophagy, and elevated activity of CDC42 compared with MSPCs of age-matched controls. Pharmacological attenuation of CDC42 activity restored function of MSPCs from mice undergoing HSCT in vitro and mitigated bone degeneration after HSCT upon in vivo treatment. Targeting dysfunctional MSPCs in the setting of allo-HSCT by attenuation of CDC42 activity might be a novel approach to ameliorate osteopenia and osteoporosis in patients receiving allo-HSCT.

Methods

Mice

For the transplantation experiments (HSCT group), we used 129Ly5.1 mice (3 months old) as donors, and 129Bl6 mice (3 months old) as recipients. Age-matched (no transplantation, middle-aged, up to 13 months) and young (129Ly5.1, 3 months old) mice were included in the experiments as control groups. To establish their age categories, we distinguished 3- to 6-month-old (young; Y) mice from 14-month-old (middle-aged; 13A) mice.[16] The mice were housed under specific pathogen–free conditions and experiments were conducted per approved ethical guidelines (Government of Upper Bavaria approvals Vet_02-14-112 et al). Further details are available in supplemental Materials.

Murine and human MSPC isolation and in vitro cell culture analysis assays

Murine long bones were flushed and crushed, followed by collagenase digestion as previously described.[11,17] After digestion, flushed or released endosteal cells were used for flow cytometry analysis and cell sorting. In the analysis and sorting of BM subpopulations we distinguished endothelial cells (ECs; $CD31^+$ $CD45/Ter119^-$), osteoblastic cells, (OBCs, $CD31^-$ $CD45/Ter119^-ALCAM^+$ $SCA1^-$), and MSPCs ($CD31^-$ $CD45/Ter119^-$ $ALCAM^{-/low}$ $SCA1^+$), as previously described.[18] The remaining bone fragments were plated (0.1% gelatin coating) and the adherent cells were cultured until passage 3 (p3; 80% confluency) in a humidified atmosphere, 5% CO_2 and at 37°C in minimal essential medium alpha with ribonucleic acids, GlutaMAX, 10% fetal calf serum, 1% penicillin-streptomycin, and 0.1% β-mercaptoethanol. Cell numbers were determined and reseeded (1×10^3 cells per cm^2) for different cell culture assays at p4, unless stated otherwise.

Human BM samples were collected with informed consent from healthy individuals (derived from the remains of stem cell transplantation bags or isolated from femoral heads after a hip surgery). Human BM samples were also obtained from allo-HSCT recipients with various malignant hematopoietic conditions. All data, both from healthy individuals and patients, were normalized and combined for analysis. Use of patient materials were approved by the institutional review board at the Technical University of Munich, School of Medicine, Munich, Germany (study TUM 538/16). Characteristics of healthy individuals and patient's treatment regimens used before allo-HSCT can be found in supplemental Table 4. Human MSPCs were cultured in low-glucose minimal essential medium alpha, supplemented with 2 mM L-glutamine, 10 U/L, and 20 U/ml penicillin-streptomycin. Freshly prepared pooled human platelet lysate, at a concentration of 10% (volume per volume), was added to the cell culture following previously described methods.[11,19]

All in vitro assays, such as fluorescence-activated cell sorting, treatment with pharmacological compounds, enumeration of CFU-F, senescence assay, immunofluorescence (IF) staining (confocal IF), as well as assessment of mitochondrial function, can be found in detail in supplemental Materials.

In vivo transplantation assay and in vivo treatment with pharmacological compounds

Whole BM cells (2.5×10^5) were IV transplanted into lethally irradiated (8.5 Gy) recipient mice, detailed in supplemental Materials. For in vitro assays, MSPCs (p4) were cultured with the Cdc42 activity-specific inhibitor (CASIN) or a vehicle (dimethyl sulfoxide) for 4 hours before starting cell culture assays. In vivo experiments were conducted using CASIN (2.4 mg/kg) or the vehicle (phosphate-buffered saline and 15% ethanol).[11] After HSCT, the compounds were administered via intraperitoneal (IP) injection every 24 hours for 4 consecutive days (day 5, 6, 7, and 8).

Micro-CT

Isolated bones were fixed in 4% paraformaldehyde in phosphate-buffered saline for 3 days and then stored in 70% ethanol. Microcomputed tomography (micro-CT) was performed and analyzed using the SkyScan1176 micro-CT scanner (supplemental Table 3). We additionally analyzed and evaluated the percent bone volume (BV) via the ratio of BV to total volume (BV/TV) by measuring only the areas that showed clear BV with ImageJ software. By setting a threshold, we focused exclusively on the dense, bright areas indicative of bone. This allowed us to selectively measure and quantify the characteristics of the bone structures.

Human BMD measurements

After allo-HSCT, patients underwent annual bone mineral density (BMD) measurements for a minimum of 5 years as per institutional guidelines. BMD was assessed via quantitative computed tomography of the lumbar spine. The quantitative CT PRO Mindways 6.1 software (https://www.qct.com/QCTPro.html) was used. Detailed

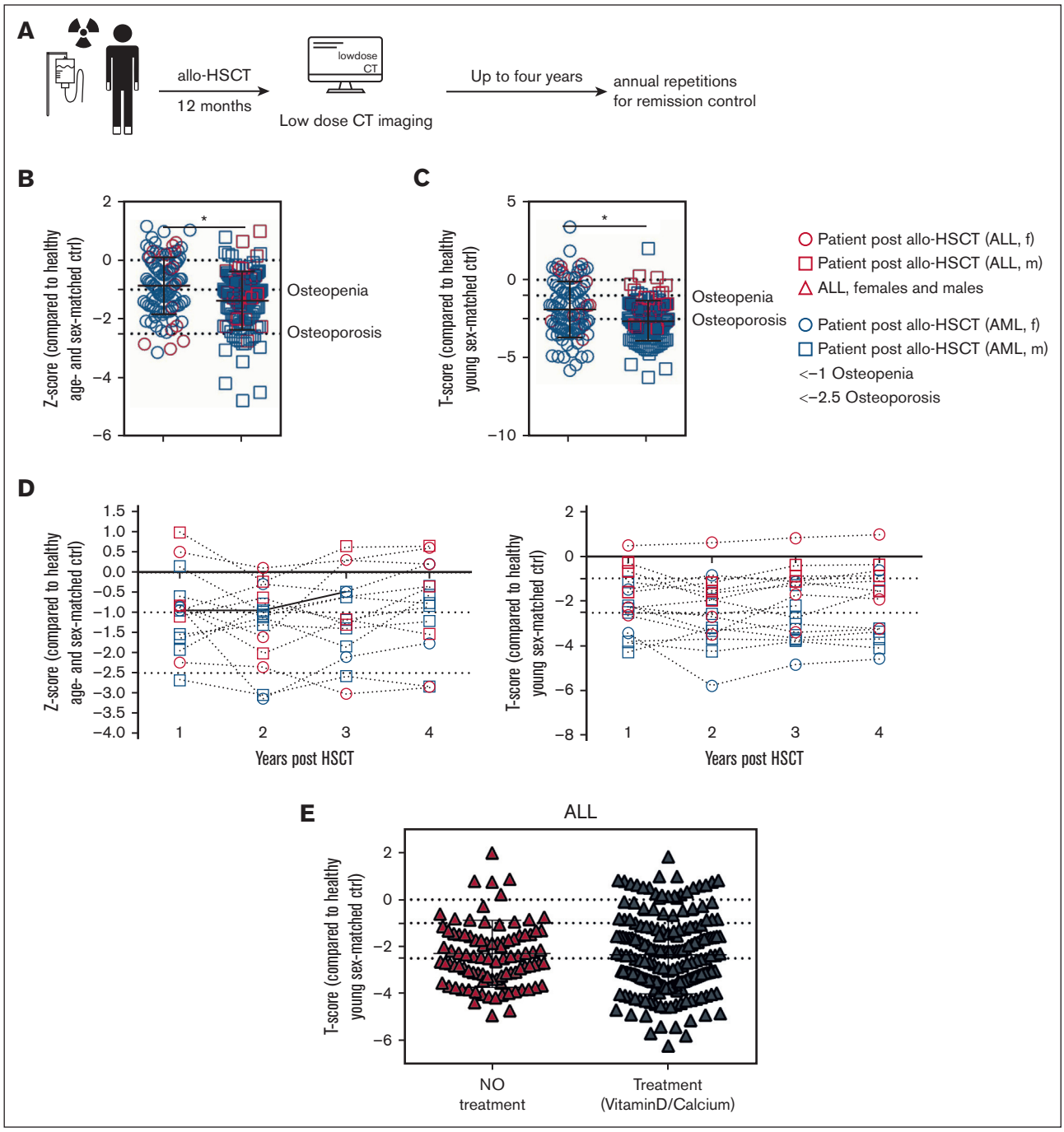

Figure 1. Human BMD measurements show induced osteoporosis after allo-HSCT. (A) Experimental design for human HSCT and myeloablation after allo-HSCT and analysis via CT 12 months after HSCT with annual repetitions for remission control (up to 4 years). Acute lymphoblastic leukemia (ALL; females, n = 17; males, n = 25) and acute myeloid leukemia (AML; females, n = 84; males, n = 97). (B) Z-score: comparison of the measured person's bone density with age- and sex-matched controls. (C) T-score: comparison of the measured person's density values with those of a healthy young adult (aged 20-30 years), comparison with peak bone density, sex matched. (D) Left graph: Z-score: comparison of the measured person's bone density with age- and sex-matched controls within the first 4 years after HSCT. Right graph: comparison of the measured person's density values with those of a healthy young adult (aged 20-30 years), comparison with peak bone density, sex-matched within the first 4 years after HSCT (right graph). (E) Analysis of differences in T-scores between vitamin D3–treated patients with Dekristol 20 0000 or calcium (calcium effervescent tablets of 500 mg) compared with untreated patients. The measurement of T- and Z-scores already incorporates BMD data across a wide age range (1-80 years) from healthy US Caucasian or Asian individuals, which constitutes a statistical analysis. *$P < .05$ (Kruskal-Wallis test: panels B,C). Data are represented as mean ± standard deviation (SD). ctrl, control; f, female; m, male.

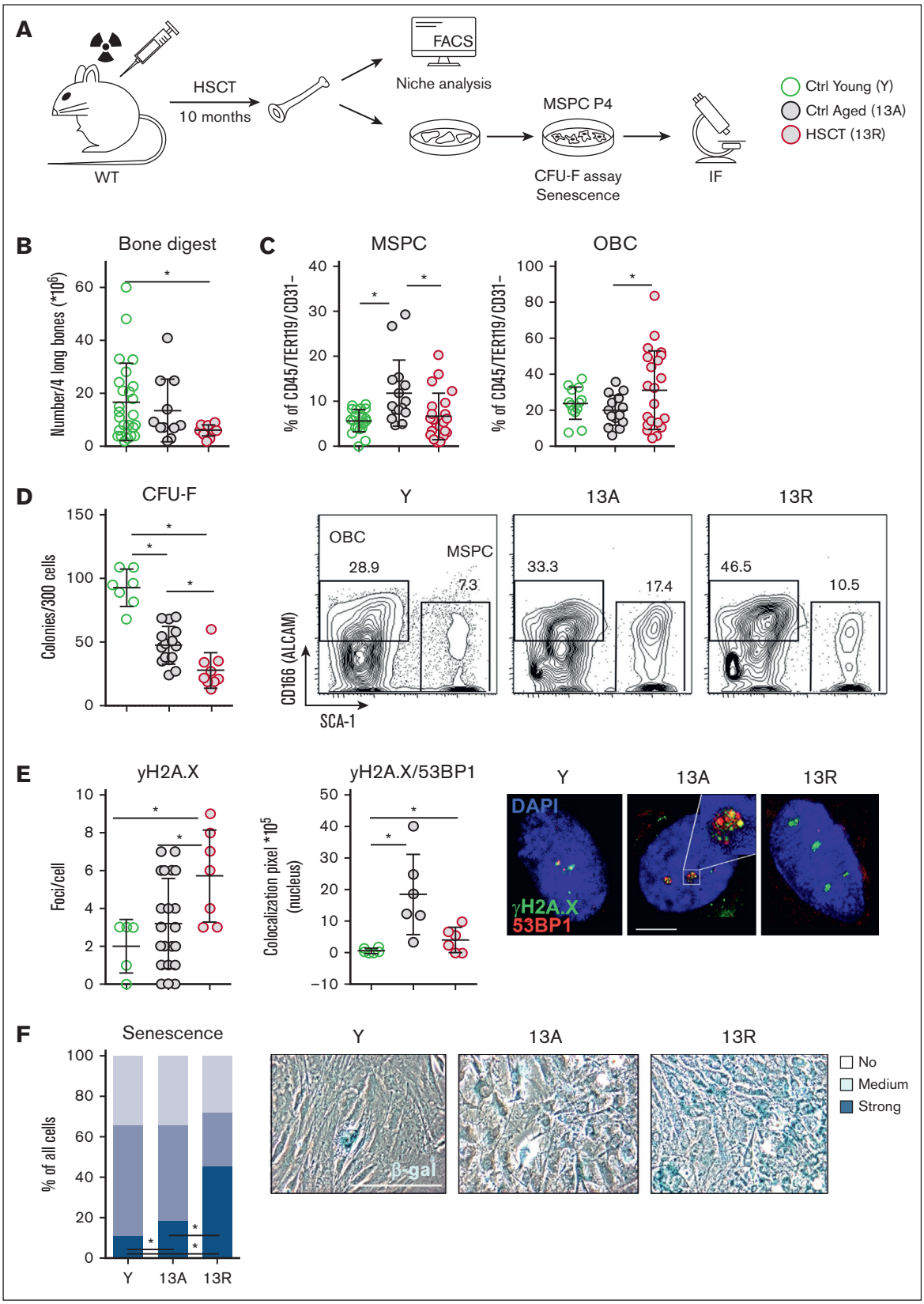

Figure 2. HSCT and permanent changes in the MSPCs. (A) Experimental design for HSCT into lethally irradiated 3-month-old wild-type mice (time point at the end of experiment: 13 months, 13R). Age-matched control group (13A) without treatment (HSCT). Analysis of the BM niche in 13-month-old mice (13A and 13R), and Y control group (3 months). Fluorescence-activated cell sorting (FACS) analysis of isolated stromal cells with subsequent cultivation of the MSPCs. (B) Graph shows the total cell number of 4

information can be found in supplemental Materials. T-scores and Z-scores were obtained retrospectively from patient records, with informed consent (ethics vote: 423/17 S).

A Z-score is used to compare an individual's bone density with the average for their age and sex, a T-score is used to compare bone density with the peak value observed in a healthy young adult. A score higher than or equal to −1 is considered normal. A value between −1 and −2.5 is referred to as osteopenia, a precursor of osteoporosis. Values lower than −2.5 is diagnosed as osteoporosis. In healthy young individuals, the Z and T-scores are typically close to 0, signifying that their bone density aligns with age and sex norms or corresponds to the peak bone density of a healthy young adult.

Bulk RNA-seq library preparation

RNA sequencing (RNA-seq) of BM MSPCs from Y, 13A, and (3 + 10) month old recipients (13R) mice was conducted using prime-sequencing based on molecular crowding SCRB-seq, with paired-end sequencing on an Illumina HiSeq1500. Detailed data processing and analysis are provided in supplemental Materials.

Statistics

Statistical analysis was conducted with Mann-Whitney tests for 2 groups, and Kruskal-Wallis tests for multiple groups, using Prism software. All statistical analyses were conducted using the Prism software package, and the results are presented as mean ± standard deviation. Detailed information can be found in supplemental Materials.

Results

A HSCT procedure results in permanent negative changes in BM-resident MSPCs

Osteoporosis is a commonly found complication in allo-HSCT.[1,2,20] More than 50% of female and 62% of male patients showed degenerative changes such as osteopenia or osteoporosis 1 year after allo-HSCT compared with healthy age- and sex-matched controls (Z-score; Figure 1A-B), and 86% of female and 91% of male allo-HSCT recipients showed clear bone loss compared with young controls (T-score; Figure 1C) in a patient cohort of the Technical University of Munich/University Hospital Klinikum rechts der Isar. Importantly, patients showed no significant improvement in bone density over time (Figure 1D) despite receiving standardized treatments such as vitamin D and calcium after transplantation, indicating that the osteoporotic changes due to HSCT may be difficult to revert (Figure 1E). To investigate the underlying mechanisms of transplant-associated long-term osteoporosis, we initially analyzed mice 10 months after the HSCT procedure.

HSCT was performed by transplanting BM cells in 3-month-old mice (young, Y) that received radiation as a preconditioning regimen. BM of the successfully reconstituted recipient animals was analyzed 10 months after HSCT (13R) to determine the long-term effect on bone-resident MSPCs ($CD31^-$ $CD45/Ter119^-$ $ALCAM^{-/low}$ $SCA1^+$) and compared with MSPCs of age-matched control mice (13A), which had not been preconditioned nor received HSCT (Figure 2A; supplemental Figure 1A). To assess the number and function of bone-forming cells after HSCT, $ALCAM^{-/low}$ MSPCs and $ALCAM^+$ $SCA1^-$ OBCs[18] were analyzed. The total number of cells from BM of 13R mice was lower than that of Y controls, whereas 13A controls were not significantly different from either Y or 13R (Figure 2B), implying successful but imperfect recovery/reconstitution of the BM in animals that underwent HSCT. Interestingly, BM showed a higher ALCAM-expressing OBC content in 13R mice than in 13A mice (Figure 2C). Next, we cultivated the MSPCs from these bones to determine their ability to generate CFU-F. The frequency of cells that were able to generate fibroblast-like colonies (CFU-F) was highest in Y MSPCs, with a diminished CFU-F frequency in the HSCT treatment and the age-matched control groups, suggesting the decline in CFU-F is time/aging related and additionally affected by HSCT (Figure 2D; supplemental Table 5). In addition, we found DNA damage in 13R MSPCs indicated by increased $\gamma H2AX^+$ double-strand break sites that are not colocalized with the DNA repair complex component 53BP1[21,22] (Figure 2E), as well as by a higher frequency of cells expressing senescence-associated β-galactosidase in 13R cultures (Figure 2F).

Altered mitochondrial quality control in MSPCs from mice undergoing HSCT

RNA-seq was performed on primary Y, 13A, or 13R MSPCs sorted from the BM (Figure 3A-B; supplemental Figure 2A-B). Comparisons between 13A and 13R MSPCs showed 257 differentially expressed genes (DEGs), 115 of which were downregulated in 13R cells (50 of those more than twofold) and 140 DEGs were upregulated (56 of which more than twofold; supplemental Figure 3C). Several of the DEGs downregulated in 13R MSPCs were genes coding for important proteins involved in mitophagy, selective autophagy, and guanosine triphosphate hydrolase (GTPase) signaling, such as ras homolog family member T1 (*Rhot1*), *Wasf2*, *Ddit3*, *Lamp1*, *Atg5*, *Tax1bp1* and *Gipc1* (Figure 3C). Further STRING (Search Tool for Retrieval of Interacting Genes/Proteins) analysis connected several of these DEGs to mitochondria-associated proteins, MYO6, parkin RBR E3 ubiquitin protein ligase (PRKN), PTEN-induced kinase 1 (PINK1), SQTSM1, and TOMM20, to possible regulation by CDC42 (Figure 3D; supplemental Figure 2D).

Figure 2 (continued) long BM flushed bones after collagenase digestion. (C) Relative numbers of immature MSPCs ($CD45/Ter119/CD31^-$ $Sca\text{-}1^+$ $Alcam^{-/low}$, left) and OBCs ($CD45/Ter1197CD31^-$ $Sca\text{-}1^-$ $Alcam^+$, right); FACS gating strategy in Landspersky et al.[11] Representative contour plots of collagenase-digested bones (below). (D) Number of colony-forming mesenchymal stem cells (CFU-F) of 300-plated cultured MSPCs (p4). (E) Graphs show foci/cell (left) and colocalization pixel of γH2A.X and 53BP1 in the nucleus of cultured MSPCs (p4; right). Representative IF images of γH2A.X (green) and 53BP1 (red) in compact bone-derived MSPCs (p4; below) counterstained with DAPI (4′,6-diamidino-2-phenylindole). (F) Average proportion of bluish β-galactosidase (β-gal)–stained compact bone–derived MSPCs (p4, left). White bar indicates cells with no detectable staining whereas light blue and dark blue refer to partially and strongly β-gal–stained cells, respectively; Y (n = 5), 13A (n = 6), and 13R (n = 4). The Kruskal-Wallis test was applied here between the 3 groups examined for each of the 3 β-gal staining concentrations (strong, medium, and no). Representative pictures of β-gal–stained MSPCs (right). The analysis represents 2-3 independent experiments. Scale bars, 5μm (E) and 20μm (F). *$P < .05$ (Kruskal-Wallis test: panels B-F). Data are represented as mean ± SD. Ctrl, control.

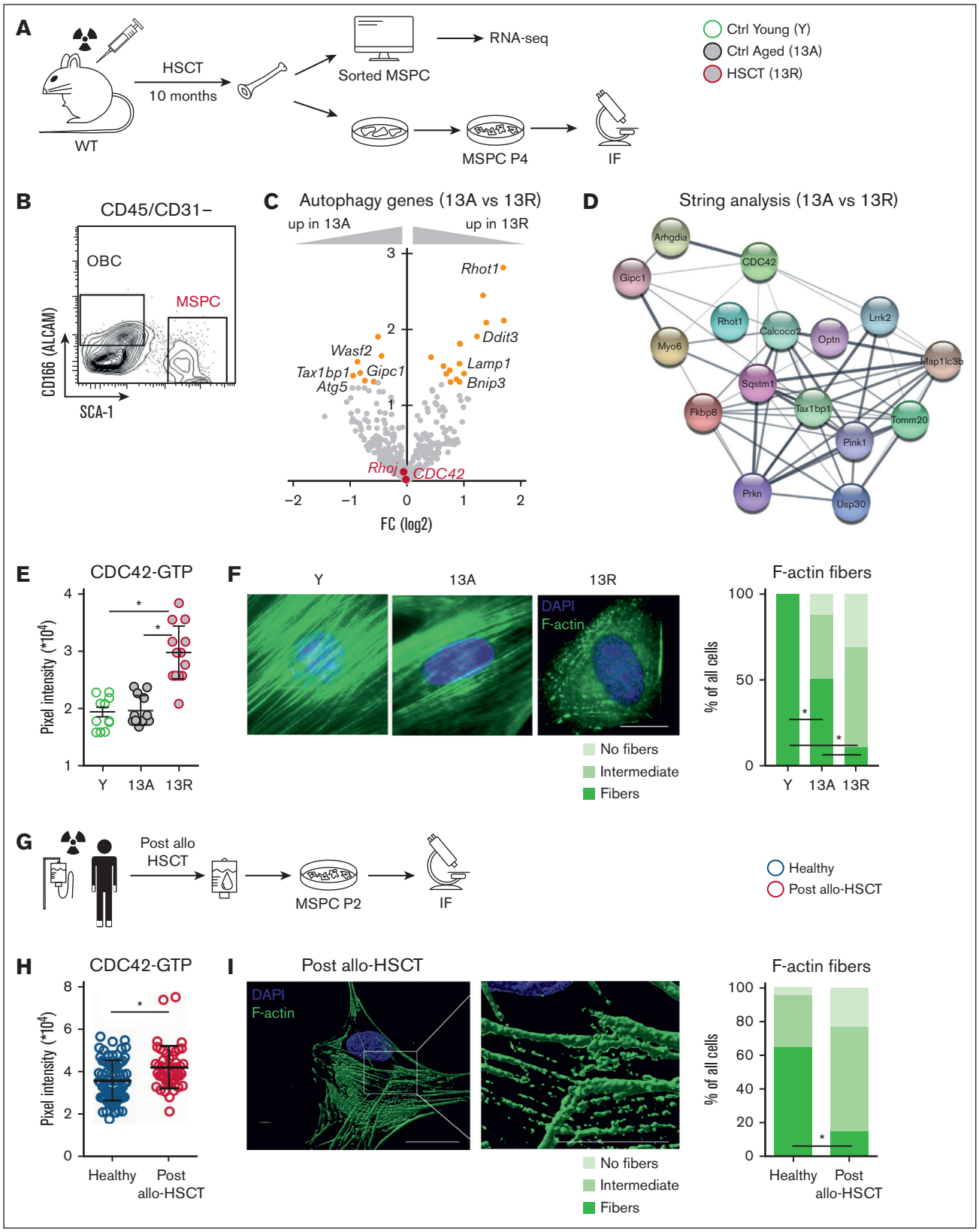

Figure 3. Impaired F-actin signaling. (A) Experimental design for HSCT into lethally irradiated 3-month-old wild-type mice (time point at the end of experiment: 13 months, 13R). Age-matched control group (13A) without HSCT. Analysis of the BM niche in 13-month-old mice (13A and 13R), and Y control group (3 months). RNA-seq analysis of sorted MSPCs (B) with subsequent cultivation of the MSPCs until p4 for analysis with IF assay. (C) Volcano plot showing differential protein expression of autophagy genes, with

The small GTPase CDC42 is a critical regulator of F-actin assembly and F-actin cages, targeting damaged mitochondria.[23,24] In addition, the fact that persistently elevated activation of CDC42 contributes to degenerative processes and aging in several different tissues,[11,25-27] led us to investigate CDC42 activity in MSPCs in more detail, first by anti–CDC42-GTP IF staining. The level of CDC42-GTP was indeed markedly upregulated in 13R MSPCs compared with both Y and 13A MSPCs (Figure 3E). In addition, MSPCs from 13R mice show significantly less elongated F-actin fibers compared with MSPCs from either Y or 13A controls (Figure 3F).

We also analyzed human MSPCs from patients with leukemia, 6 to 24 months after receiving allo-HSCT and who were within complete remission and compared them to MSPCs from hematologically healthy aged-matched controls (Figure 2G; supplemental Figure 1B). The allo-HSCT recipients were conditioned before transplantation, either by total body irradiation (2 patients) or by chemotherapy (5 patients; supplemental Table 4). As in mice, we found high levels of active CDC42-GTP as well as less elongated F-actin fibers in MSPCs from these donors compared with MSPCs from healthy age-matched controls (Figure 3H-I). In addition, also the human MSPCs from the transplant recipients showed a larger proportion of senescent cells (supplemental Figure 2F). In summary, also human MSPCs from patients that underwent allo-HSCT show changes associated with premature aging, like murine MSPCs in transplant recipients.

Damaged mitochondria are marked for mitophagy, but not cleared, in 13R MSPCs

Damaged mitochondria are targeted for mitophagy by F-actin.[23,24] Changes in the F-actin fiber length in MSPCs from transplant recipients (Figure 3I) might therefore affect mitophagy. Costaining of F-actin and mitochondria (via TOMM20, a protein localized on the outer membrane of mitochondria) revealed F-actin encapsulated mitochondria in 13A MSPCs, and even stronger in 13R MSPCs, whereas in Y MSPCs the mitochondria were not directly surrounded by F-actin fibers (Figure 4A-B). Furthermore, we detected increased reactive oxygen species (ROS) production in 13R MSPCs (supplemental Figure 3A-B), indicative of an increase in damaged mitochondria.[28] These findings are in line with a view that damaged mitochondria are encapsulated in 13R MSPCs but do not seem to be cleared. RHOT1 (also known as MIRO-1) identifies damaged mitochondria.[29] Colocalization experiments showed RHOT1 was strongly colocalized with TOMM20$^+$ mitochondria in both 13A and 13R MSPCs compared with Y controls (Figure 4C), indicating that damaged mitochondria are marked by RHOT1 in these cells. The motor-cargo protein MYO6 anchors mitochondria marked with RHOT1 to F-actin.[23,30] Our experiment showed that MYO6 colocalized at high levels with TOMM20$^+$ mitochondria in 13A and 13R MSPCs (Figure 4D), indicating that the RHOT1-MYO6 complex marked the damaged mitochondria. In contrast, MYO6 did not colocalize at all to F-actin in 13R but colocalization was detected in 13A MSPCs (Figure 4E; supplemental Figure 3C). Our results are consistent with a view that damaged mitochondria are recognized and encapsulated into F-actin cages in both 13A and 13R MSPCs, however, in 13R MSPCs, the mitochondria are not connected to F-actin for transport, a critical requirement for clearance of damage mitochondria.

The disruption of the final steps in mitophagy noted in 13R cells may also be relevant to MSPC fate. The selective autophagy receptors interact with MYO6,[23,31] and less OPTN has been associated with osteoporosis.[15] In our experiments, expression of OPTN is indeed reduced in 13R vs 13A MSPCs (Figure 4F).

Improving the regeneration of MSPCs by targeting CDC42 activation in vitro

Our data imply altered F-actin biology in 13R MSPCs, which are likely linked to altered clearance of mitochondria. We, and others, have shown that a defective F-actin fiber orientation in stressed cells is, at least partly, due to elevated activation of CDC42.[25-27] Attenuation of this CDC42 activation by a CASIN can restore the function of acutely stressed MSPCs.[11] Because CDC42-GTP levels were also elevated in both murine and human MSPCs from transplant recipients (Figure 3E-H), we therefore tested whether attenuation of CDC42 activity in HSCT MSPCs could rescue changes in the MSPCs, restore the transport of damaged mitochondria to mitophagosomes, and reverse the impaired function of 13R MSPCs.

In vitro treatment of 13R MSPCs with CASIN indeed restored alterations in the local environment, such as increased cell senescence and γH2A.X-directed DNA damage repair mechanisms (Figure 5A-C; supplemental Figure 4A-B). In addition, the in vitro treatment reduced CDC42-GTP levels and restored both F-actin levels and fiber formation, as well as mitochondrial diameter and actin cages (Figure 5D-F; supplemental Figure 4C-E). Treated MSPCs show a reconnection of F-actin and MYO6 (Figure 5G).

Figure 3 (continued) adjusted *P* values (false discovery rate [FDR]) plotted against $\log_2$ fold change (FC). 13A, n = 10 and 13R, n = 7. The dark dots show proteins that meet the FDR threshold for statistical significance (FDR < 0.05) and are considered differentially expressed. (D) Analysis of the DEGs using STRING (Search Tool for Retrieval of Interacting Genes/Proteins) for visualizing an interaction network. (E) Graph shows the protein content of CDC42-GTP in cultured MSPCs (p4). (F) Left: representative IF images of MSPCs (p4). IF staining of F-actin (green) counterstained with DAPI (blue). Right: evaluation of the orientation of F-actin fibers stained with phalloidin. Percentage of all cells showing fibers (bar in dark green), intermediate oriented fibers (bar in bright green), or no stress fibers (white bar). The Mann-Whitney test was applied here between the 3 groups examined for each of the 3 stress fiber orientations (fibers, intermediate, and no fibers). (G) Experimental design for human HSCT and myeloablation via chemotherapeutics (n = 5) or irradiation (n = 2) and analysis from 6 months up to 24 months after HSCT in human BM samples. Healthy donor samples as controls (n = 6). (H) Graphs show the protein content of CDC42-GTP measured by ImageJ software from healthy age-matched controls (n = 6) and allo-HSCT recipient (n = 7; left). (I) Left: representative IF staining of F-actin (green; right) counterstained with DAPI (blue) of a patient sample after allo-HSCT. Right: evaluation of the orientation of F-actin fibers stained with phalloidin. Percentage of all cells showing fibers (bar in dark green), intermediate oriented fibers (bar in bright green pattern), or no fibers (white bar). The Mann-Whitney test was applied here between the 3 groups examined for each of the 3 fiber orientations (fibers, intermediate, and no fibers). The analysis represents 2-3 independent experiments except for the RNA-seq analysis, which was performed once with a high number of samples (Y, n = 9; 13A, n = 10; and 13R, n = 7). Scale bars, 10 μm. *$P < .05$ (Kruskal-Wallis test, panel E,H; F-actin fibers/intermediate/no fibers were either present [value = 1], or not [value = 0]). Only the results for the presence of elongated F-actin fibers are presented in panels F and I and analyzed with the nonparametric Mann-Whitney test. Data are represented as mean ± SD.

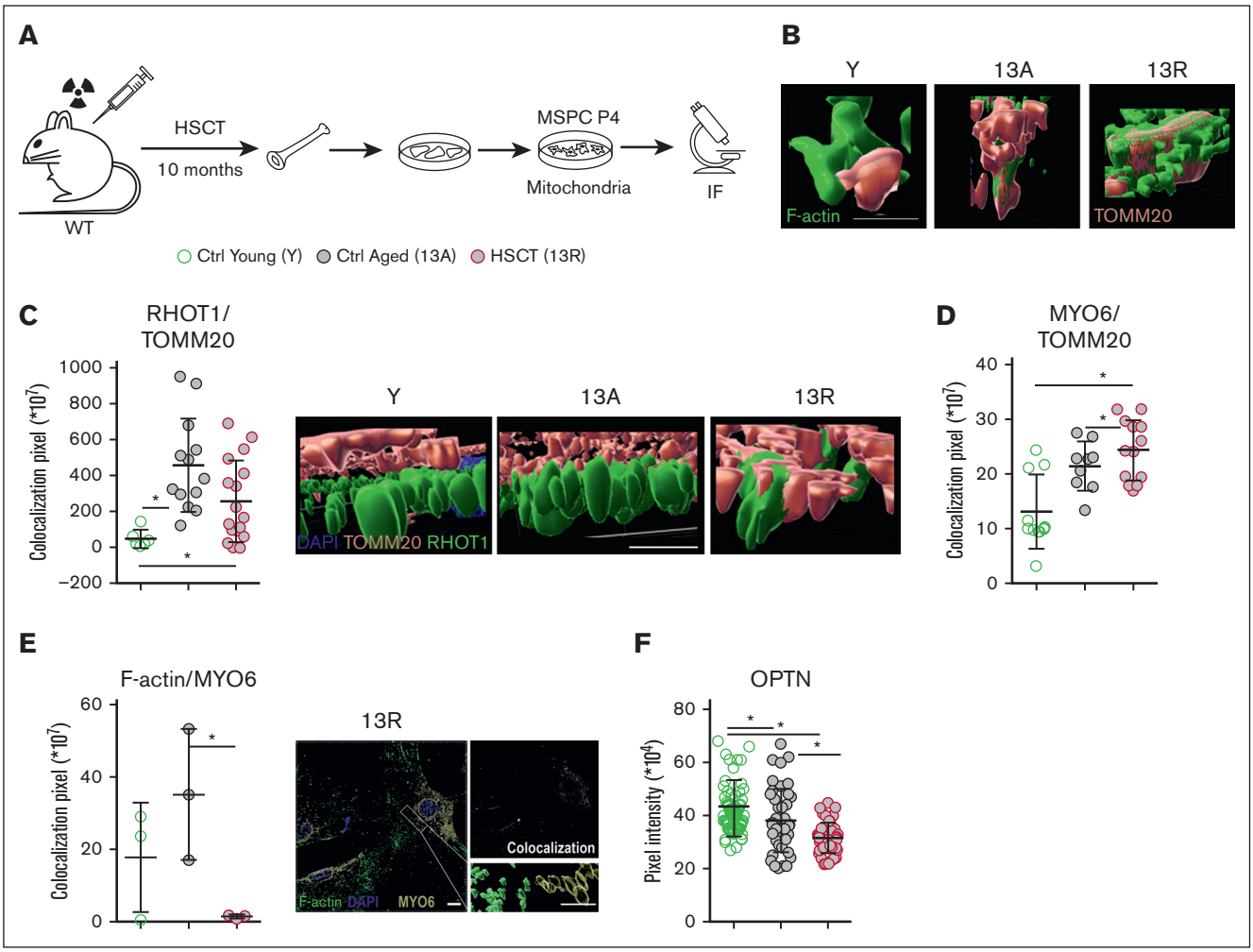

Figure 4. Damaged mitochondria in MSPCs of HSCT-mice. (A) Experimental design for HSCT into lethally irradiated 3-month-old wild-type mice (time point at the end of experiment: 13 months, 13R). Age-matched control group (13A) without HSCT. Analysis of the BM niche in 13-month-old mice (13A and 13R), and Y control group (3 months). Analysis of cultured MSPCs until p4 for analysis with IF assay. (B) Representative confocal microscopy images stained for F-actin (green) and TOMM20 (red) in MSPCs (p4). Image section of a mitochondrion with actin cages. (C) Colocalization pixel of RHOT1 and TOMM20 measured by ImageJ software (left) and representative confocal microscopy images of RHOT1 (green) and TOMM20 (red) counterstained with DAPI (blue, right). (D) Colocalization pixel of MYO6 and TOMM20 measured by ImageJ software. (E) Colocalization pixel of MYO6 and F-actin measured for 3 cells with Imaris software (left) and representative confocal microscopy images for F-actin (stained in green) and MYO6 (yellow) counterstained with DAPI (blue) with additional visualization of colocalization (white) in MSPCs of 13R mice (P4, right). (F) Protein content of OPTN of MSPCs (p4) measured by ImageJ software (the analysis represents 2-3 independent experiments). Scale bars (mitochondria), 0.2µm; scale bars (nucleus), 10 µm. *$P < .05$ (Kruskal-Wallis test: panels C-F). Data are represented as mean ± SD.

Conversely, where RHOT1 encapsulates mitochondria in 13R MSPCs (Figure 4C), CASIN treatment strongly reduces binding of RHOT1 to TOMM20 indicating either that the treatment interferes with RHOT1 binding or that mitochondria are normally cleared resulting in smaller and functional mitochondria (supplemental Figure 4F). These in vitro treatment experiments indicate that CASIN might repair mitochondrial quality control in 13R MSPCs by reconnecting MYO6 with now again elongated F-actin fibers. This suggests a reversal of the disrupted mitophagy process and suggests a return to a healthier, more functional state of mitochondria in 13R MSPCs after CASIN intervention. Additionally, we investigated whether RHOT1 colocalized with LAMP1, demonstrating that mitophagolysosome formation is possible in 13A and 13R after in vivo CASIN treatment. Whereas without treatment, we observed low levels of RHOT1/LAMP1 colocalization, CASIN treatment increased colocalization in 13A and 13R MSPCs compared with the Y control group (Figure 5H; supplemental Figure 4G). This finding supports the idea that CASIN treatment promotes the clearance of RHOT1-marked mitochondria via mitophagy in these experimental groups.

Attenuation of CDC42 activity in vivo after HSCT prevents osteoporotic changes

For testing the effects of attenuation of CDC42 activity in vivo in animals that underwent HSCT, we chose a treatment regimen in which CASIN was injected IP on 4 consecutive days on day 5 through 8 after HSCT (day 0), and animals were again monitored

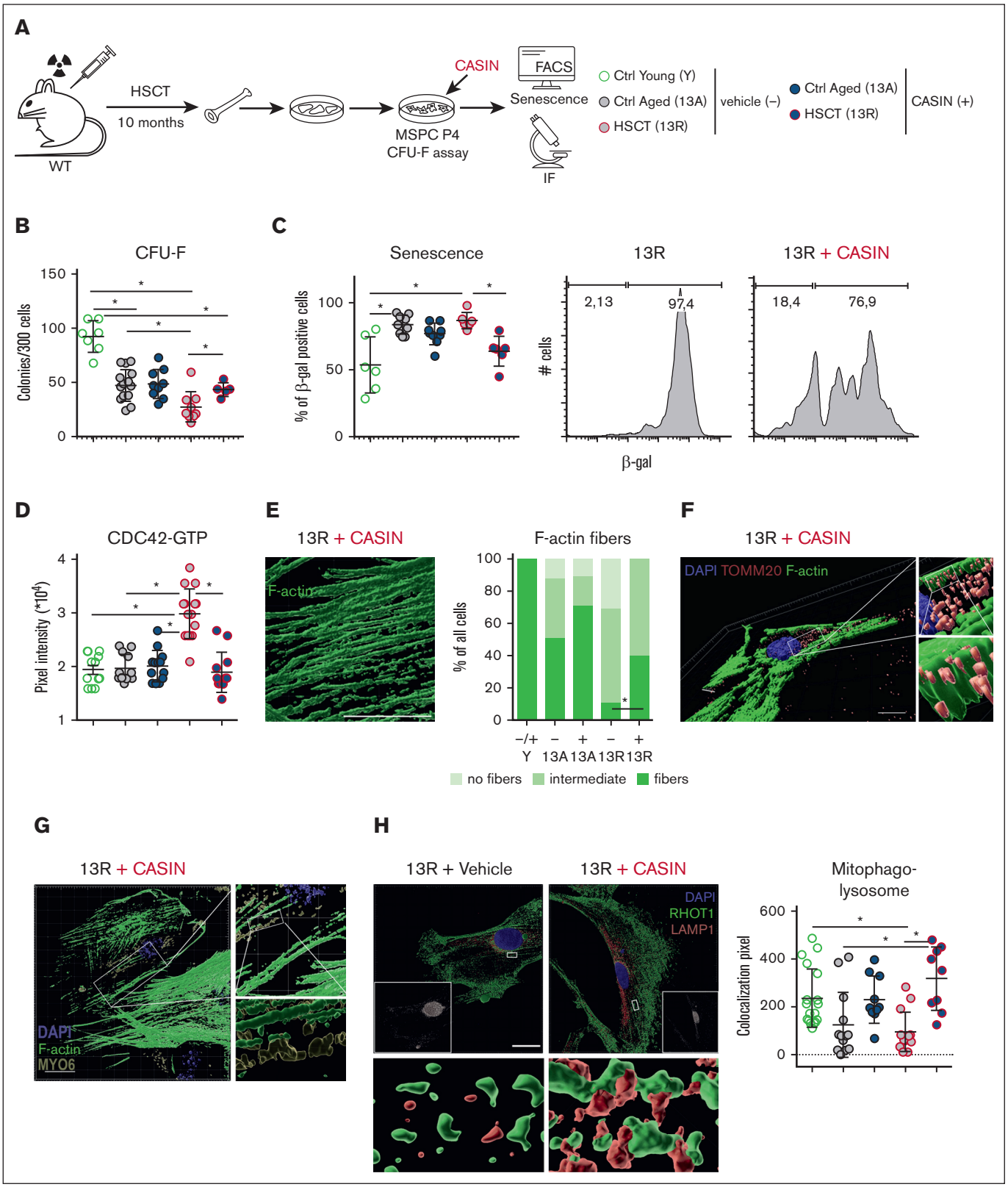

Figure 5. Pharmacological treatment rescues changes in the microenvironment and mitophagy in MSPCs in vitro. (A) Experimental design for HSCT into lethally irradiated 3-month-old wild-type mice (time point at the end of experiment: 13 months, 13R). Age-matched control group (13A) without HSCT. Analysis of the BM niche in 13-month-old mice (13A and 13R), and Y control group (3 months). MSPC culture and CASIN (blue filled symbols) or vehicle (dimethyl sulfoxide, gray-filled symbols) treatment in vitro at p4. (B) Number of colony-forming mesenchymal stem cells (CFU-F) of 300 plated cultured MSPCs (p4). (C) Average proportion of β-gal positive–stained compact

10 months after transplant (Figure 6A). In vivo application of CASIN reduces the activity of CDC42 in vivo in BM cells.[11] First, the elevated BM OBC numbers that were associated with 13R animals returned in 13R + CASIN mice to levels seen in 13A mice (Figure 6B). Functional assays show that 10 months after HSCT, MSPCs show an increase in damaged mitochondria, indicated by elevated ROS levels and low tetramethylrhodamine methyl ester staining (Figure 6C-D). Interestingly, by short in vivo CASIN treatment administered 10 months before analysis, ROS levels were significantly reduced, and the membrane potential recovered in MSPCs. Next, we analyzed femora to determine macro(cortical)- and micro(trabecular)-structural parameters using micro-CT (Figure 6A). This analysis showed that BV/TV was reduced in the femurs of HSCT animals. Importantly, CASIN administration in vivo markedly improved BV/TV to the levels of young and age-matched controls (Figure 6E). The trabecular and cortical microarchitecture was significantly improved in 13R + CASIN femora. Furthermore, there was significantly elevated trabecular thickness in 13R + CASIN animals than 13A and 13R bones, and significantly elevated cortical thickness in 13R + CASIN animals than 13A animals (Figure 6F-G). Interestingly, CASIN treatment within the age-matched control group showed the same effects (supplemental Figure 5A-D). In summary, pharmacological targeting of CDC42 activity in vivo after HSCTs might attenuate unwanted, likely preconditioning-associated, changes in MSPCs and bones.

Discussion

Our study highlights long-term effects of ablative conditioning with subsequent BM transplantation (HSCT). Although changes in bone remodeling and bone turnover induced by HSCT over time have been reported by others, details of the underlying mechanisms are incompletely understood. Our findings demonstrate that post-HSCT MSPCs show markedly reduced proliferation and increased number of committed MSPCs, coupled with cellular senescence, persisting DNA and mitochondrial damage, and reduced F-actin orientation. Although mitochondrial function has been described to be critical for the regenerative capacity of HSCs,[32,33] the role of such processes for the function of post-HSCT MSPCs is poorly studied.

Our results are in line with recent data showing that MSPC mitochondria respond to stressors by undergoing fusion, followed by fission, and finally mitophagy, which contributes to the osteogenic differentiation process.[34,35] This sequence of events is disrupted in 13R MSPCs, in which oxidative stress is elevated, fission and mitophagy are reduced, likely contributing to HSCT-associated osteoporosis. It appears from our experiments that HSCT aggravates mitophagy in such a manner that selective degradation of dysfunctional mitochondria is strongly reduced. In sum, these observations suggest that accumulation of damaged mitochondria and the accompanying oxidative stress supports the osteoporotic decrease in bone mass,[36] a hypothesis further supported by our evaluation of yearly checkup data from allo-HSCT patients. The patient data further show that in human allo-HSCT recipients, osteoporotic changes in bone mass persist, despite treatments of the secondary osteoporosis. These findings propose that osteoporotic remodeling after allo-HSCT is irreversible. Considering this, our experiments favor the point of view that initiating treatment prior to the diagnosis of osteopenia or osteoporosis, independent of risk factors, may be relevant for the clinical management of HSCT patients to prevent or repair anticipated osteoporotic changes.

We, and others, have found that attenuation of CDC42 activity has major effects on the F-actin[11,37] and tubulin[25] cytoskeleton. Both cytoskeletal components are critical for cellular maintenance processes, such as autophagy and vesicle transport. Clearance of damaged mitochondria is thought to be initiated by recognition of damaged mitochondria by a complex of RHOT1, PINK1, and PRKN,[38] which binds to selective autophagy receptors[39] as well as recruits so-called actin cages through binding to the MYO6 motorprotein.[23] CDC42 is involved in this process, because it triggers the necessary actin nucleation.[40] In our experiments, we found that in post-HSCT MSPCs, CDC42 is persistently overactivated and desensitized to stimuli, suggesting aging-like functional disruption as previously noted in HSCs[25] and other cell types.[26,27]

Previous studies found that both cytostatic- or irradiation-mediated myeloablation, causes bone loss.[41] To mitigate bone loss, therapies have been proposed to reduce osteoclast activity, or may increase osteoblast function.[42] Early studies showed that bisphosphonates, which are calcium-chelating molecules,[43] effectively inhibit osteoclast-mediated bone resorption.[44] Moreover, bisphosphonates also act to reduce prenylation and, by doing so, inhibit membrane trafficking of small GTPases, including CDC42,[45] as a result of which activated CDC42 may accumulate. The effects of bisphosphonates on HSCs or the hematopoietic niche are, however, controversially discussed, for which positive effects on CFU-F frequency,[46,47] no effects on HSCs,[41] as well as deleterious effects on HSCs,[48] B-lymphopoiesis,[49] and MSPCs have

Figure 5 (continued) bone–derived MSPCs (p4, left). Representative FACS plots for β-gal–positive 13R with or without CASIN MSPCs. (D) Protein content of CDC42-GTP measured with ImageJ software. (E) Left: representative F-actin staining in cultured 13R + CASIN MSPCs (phalloidin, green). Evaluation of the orientation of F-actin fibers stained with phalloidin. Right graph: percentage of all cells showing fibers (bar in dark green), intermediate oriented fibers (bar in bright green), or no fibers (white bar). The Mann-Whitney test was applied here between all groups examined for each of the 3 fiber orientations (fibers, intermediate, and no fibers). For a better overview, not all significant values are shown. Some of them (without/no CASIN treatment) are already shown in Figure 3F. In addition, the following groups are significant: *Y vs 13A+; Y vs 13R+; 13A+ vs 13R+. (F) Representative confocal microscopy images stained for F-actin (green) and TOMM20 (red) counterstained with DAPI (blue) of 13R MSPCs (p4) with and without CASIN treatment. Image section of mitochondria embedded in actin structure. (G) Representative confocal microscopy images for F-actin (stained in green) and MYO6 (yellow) in MSPCs of 13R mice (p4) with and without CASIN treatment. (H) Left: representative confocal microscopy images for RHOT1 (stained in green) and LAMP1 (red) in MSPCs of 13R mice (p4) with and without CASIN treatment. Colocalization is shown in white. Right graph: colocalization pixel of RHOT1 and LAMP1 measured by ImageJ software. The analysis represents 2-3 independent experiments. Scale bars (mitochondria), 0.2μm; Scale bars (nucleus), 10μm. *$P < .05$ (Kruskal-Wallis test: panels B,C,D,H; F-actin fibers/intermediate/no fibers were either present [value = 1], or not [value = 0]). Only the results for the presence of elongated F-actin fibers are presented in panel E and analyzed with the nonparametric Mann-Whitney test. Data are represented as mean ± SD. Y, young; A+, aged 13 months with CASIN (=13A+); 13R+, regenerated 13 months with CASIN.

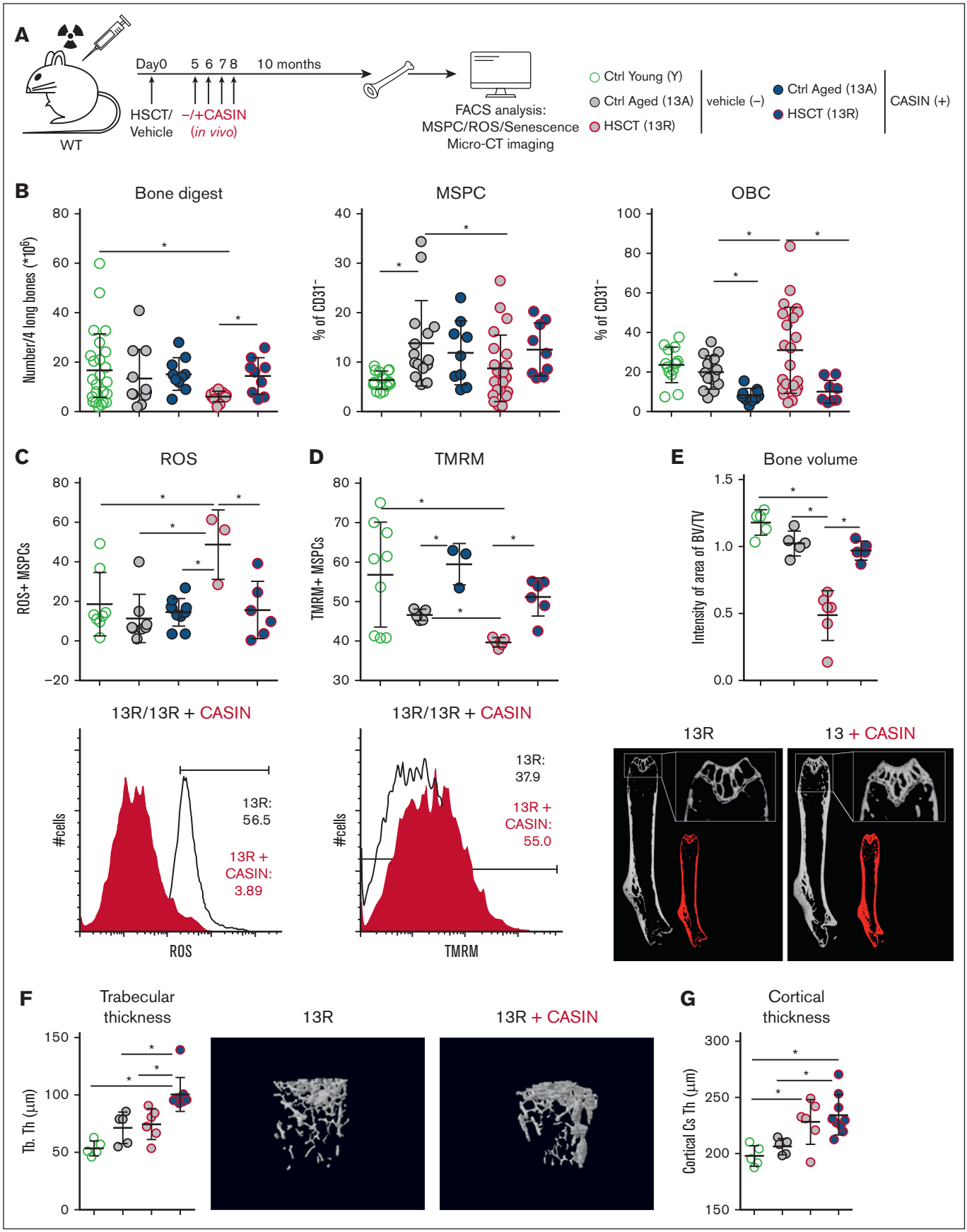
A
WT
Day0
5 6 7 8
10 months
HSCT/
Vehicle
–/+CASIN
(in vivo)
FACS analysis:
MSPC/ROS/Senescence
Micro-CT imaging
Ctrl Young (Y)
Ctrl Aged (13A)
HSCT (13R)
vehicle (–)
Ctrl Aged (13A)
HSCT (13R)
CASIN (+)
B
Bone digest
Number/4 long bones (*10^6)
MSPC
% of CD31−
OBC
% of CD31−
C
ROS
ROS+ MSPCs
D
TMRM
TMRM+ MSPCs
E
Bone volume
Intensity of area of BV/TV
13R/13R + CASIN
#cells
13R:
56.5
13R +
CASIN:
3.89
ROS
13R/13R + CASIN
#cells
13R:
37.9
13R +
CASIN:
55.0
TMRM
13R
13 + CASIN
F
Trabecular
thickness
Tb. Th (µm)
13R
13R + CASIN
G
Cortical
thickness
Cortical Cs Th (µm)

Figure 6.

been reported.[47,49] These side effects may limit the use of bisphosphonates in HSCT recipients, the recommended therapy for secondary osteoporosis after HSCT.[50]

Because osteoporotic changes are a frequent and seemingly irreversible complication, exacerbated in allo-HSCT because of more aggressive conditioning, chronic graft-versus-host disease (GVHD) and prophylactic steroid treatment,[51,52] research of additional therapeutics to treat secondary osteoporotic changes by stimulating osteogenic cells are being pursued.[53] Several of these agents have entered clinical trials, in which side effects such as gastrointestinal disorders, hypercalcemia, and osteonecrosis of the jaw are frequently noted.[53] Additional preclinical studies target myeloablation-induced senescence[54] using proteasome inhibition,[55,56] and our experiments add that early treatment to attenuate CDC42 activation positively affects both BV and trabecular thickness of femoral bones. Our studies may facilitate additional possibilities to treat osteoporotic changes after HSCT using a single agent or in combination with existing therapies.

Whereas bisphosphonates target prenylation and thereby act indiscriminately on many small GTPases, CASIN specifically inhibits the RhoGDI/CDC42 complex,[57] leaving other small GTPases unaffected. Considering that CDC42-GTP accumulates in different cell types with age, the use of CASIN may particularly benefit older HSCT recipients. We demonstrate that CDC42-GTP is upregulated in MSPCs, and reduced in CASIN-treated HSCT recipients. This appears to contradict reports in which bisphosphonates inhibit prenylation and promote CDC42-GTP accumulation in myeloid cells.[45] In contrast, because CDC42 is a central component of the noncanonical Wnt pathway, our findings support the use of anti-Wnt signaling therapies, such as antisclerostin therapy, which reduces osteoporosis by reducing osteoblast apoptosis after radiation.[58]

By administering CASIN immediately after HSCT, we adopted a treatment schedule that could feasibly be developed for HSCT protocols, with many patients being middle-aged to advance-aged and the treatment could be performed while stationary from the HSCT procedure. It is tempting to speculate that CASIN treatment either prevents osteoporotic changes or may partly reverse an already existing osteoporosis as well as further secondary side effects on MSPCs resulting from patient conditioning, not only in HSCT procedures but also in other cancer treatments.

Limitations of this study

Our in vitro and in vivo experiments focus on CDC42 activation as a therapeutic target for supporting osteogenic MSPCs. As such, we have not included an in-depth analysis of osteoclasts and their bone-resorbing activity. It is highly likely, however, that IP-injected CDC42 activity modulators will not only affect MSPCs of the BM but will also act on many other cells, including osteoclasts. In particular, bone resorption relies on the formation of actin rings, which, in turn, require CDC42 activation for assembly of the ARP2/3 actin nucleation complex.[59] Thus, it would be interesting to study in the future how the (dis)balance between bone formation by osteoblasts and bone resorption by osteoclasts is affected by attenuation of CDC42 activity in murine and human HSCT-derived cells.

Furthermore, congenic transplantation in mice does not match all aspects and complications in clinical allo-HSCT, and it is likely that immunosuppression, for example with corticosteroids, and GVHD, contribute to disrupted bone homeostasis in humans. In addition, osteoporotic changes after allo-HSCT are, in general, more severe than those observed in autologous HSCT.[51,52] However, late toxicities of autologous HSCT are driven by the drugs used for conditioning, which historically include busulfan and, for acute lymphoblastic leukemia, also total body irradiation, indeed similar to allo-HSCT. Indeed, 1 study finds that reduced BMD is found with similar incidence and severity in autologous HSCT and allo-HSCT in the absence of steroid use.[60]

In our view, these reported findings further highlight the potential benefit of CASIN treatment for preventing or reducing osteogenic degeneration, particularly in allo-HSCT recipients with GVHD and/or prolonged immunosuppressive therapy. Examining the additional role of GVHD and immunosuppression in mediating the observed effects is, however, beyond the scope of our study but will certainly need to be considered in future translational work with GVHD mouse models.

Acknowledgments

The authors thank Matthias Schiemann, Lynette Henkel, Immanuel Andrä, Corinne Angerpointner, and Susanne Dürr (Flow Cytometry Core Unit Technical University of Munich) for cell sorting. The authors also thank Ann-Engel Timm and Linda Cäsar for helping with experiments.

Figure 6. In vivo pharmacological treatment accompanying transplantation process rescues bone biology in mice. (A) Experimental design for HSCT into lethally irradiated 3-month-old wild-type mice (time point at the end of experiment: 13 months, 13R). Age-matched control group (13A) without HSCT. In vivo injection of CASIN (IP, blue filled symbols) at days 5, 6, 7, and 8 after HSCT (13R). Vector injection (phosphate-buffered saline and 15% ethanol, gray-filled symbols) at the same time points. Analysis of the BM niche of 13-month-old mice (13R with or without CASIN and 13A with or without CASIN) and Y control group (3 months, no HSCT; no CASIN and/or vehicle treatment). CT imaging of young and 13-month-old mice (13R + CASIN, 13R + vehicle, and 13A (13A no HSCT; no CASIN and/or vehicle treatment). (B) Graph shows the total cell number out of 4 long BM flushed bones after collagenase digest with CASIN or vehicle treatment (left graph) and relative numbers of immature MSPCs (CD45/Ter119/CD31$^-$ Sca-1$^+$ Alcam$^{-/low}$, middle left) and OBCs (CD45/Ter119/CD31$^-$ Sca-1$^-$ Alcam$^+$, middle right). (C) Graph shows ROS (reactive oxygen levels) staining measured with FACS analysis in cultured MSPC (p4) with representative FACS plot (right). 13R + vehicle, black; 13R + CASIN, red. (D) Graph shows tetramethylrhodamine methyl ester (mitochondrial membrane potential) staining measured with FACS analysis in cultured MSPC (p4) with representative FACS plot (right). 13R + vehicle, black; 13R + CASIN, red. (E) Micro-CT image of 1 dissected long bone (femur) per mouse (all males). Percentage of BV relative to total volume (TV, graph left) measured with ImageJ software and representative micro-CT images of 13R + CASIN (right). (F) Trabecular thickness analyzed with micro-CT imaging with representative micro-CT image of trabecular structures in mouse femur of 13R + CASIN (right). (G) Cortical thickness analyzed with micro-CT imaging. The analysis represents 2-3 independent experiments. The micro-CT imaging was performed once. *$P < .05$ (Kruskal-Wallis test: panels B-G). Data are represented as mean ± SD. Cs.Th, cortical thickness; PB, peripheral blood; Tb.Th, trabecular thickness.

This study was funded by the German Research Foundation (DFG; grants FOR 2033 [project B3], OO 8/18 and OO 8/21 [R.A.J.O.]). K.S.G received funding from the European Research Council under the European Union's Horizon 2020 Marie Sklodowska-Curie Innovative Training Network (grant agreement no. 953407).

Authorship

Contribution: T.L., J.G., R.A.J.O., and C.S. designed experiments and interpreted results; T.L., J.G., M. Saçma, M. Stein, K.B., J.S.H., F.H., S.R.M., E.S., and C.S. performed experiments and collected data; J.R., E.H., D.R., J.T., F.B., M.V., P.H., K.S.G., H.G., and W.E. contributed vital reagents and analytical tools; T.L., J.G., M. Saçma, M. Stein, J.R., B.V., R.A.J.O., and C.S. analyzed and interpreted data and performed statistical analyses; and T.L., R.A.J.O., and C.S. wrote the manuscript.

Conflict-of-interest disclosure: The authors declare no competing financial interests.

ORCID profiles: T.L., 0009-0001-7323-5113; M.S., 0000-0003-2926-6219; J.G., 0000-0002-5070-3404; K.B., 0000-0003-4028-5357; J.R., 0000-0002-4680-2071; B.V., 0000-0002-1084-7067; J.T., 0000-0003-3691-275X; J.S.H., 0000-0002-1531-0517; K.S.G., 0000-0002-6276-8002; W.E., 0000-0002-4056-0550; H.G., 0000-0002-5794-5430; R.A.J.O., 0000-0002-4947-0412; C.S., 0000-0002-0377-1412.

Correspondence: Christina Schreck, Department of Internal Medicine III, Klinikum rechts der Isar, Technische Universität München, Ismaningerstrasse 22, 81675 München, Germany; email: christina.schreck@tum.de; and Robert A. J. Oostendorp, Department of Internal Medicine III, Klinikum rechts der Isar, Technische Universität München, Ismaningerstrasse 22, 81675 München, Germany; email: robert.oostendorp@tum.de.

References

1. Schimmer AD, Mah K, Bordeleau L, et al. Decreased bone mineral density is common after autologous blood or marrow transplantation. *Bone Marrow Transplant*. 2001;28(4):387-391.
2. Schimmer AD, Minden MD, Keating A. Osteoporosis after blood and marrow transplantation: clinical aspects. *Biol Blood Marrow Transplant*. 2000;6(2A):175-181.
3. Savani BN, Donohue T, Kozanas E, et al. Increased risk of bone loss without fracture risk in long-term survivors after allogeneic stem cell transplantation. *Biol Blood Marrow Transplant*. 2007;13(5):517-520.
4. Inamoto Y, Lee SJ. Late effects of blood and marrow transplantation. *Haematologica*. 2017;102(4):614-625.
5. Qadir A, Liang S, Wu Z, Chen Z, Hu L, Qian A. Senile osteoporosis: the involvement of differentiation and senescence of bone marrow stromal cells. *Int J Mol Sci*. 2020;21(1):349.
6. Frobel J, Landspersky T, Percin G, et al. The hematopoietic bone marrow niche ecosystem. *Front Cell Dev Biol*. 2021;9:705410.
7. Cai Y, Song W, Li J, et al. The landscape of aging. *Sci China Life Sci*. 2022;65(12):2354-2454.
8. Zhong L, Yao L, Tower RJ, et al. Single cell transcriptomics identifies a unique adipose lineage cell population that regulates bone marrow environment. *Elife*. 2020;9:e54695.
9. Mo C, Guo J, Qin J, et al. Single-cell transcriptomics of LepR-positive skeletal cells reveals heterogeneous stress-dependent stem and progenitor pools. *EMBO J*. 2022;41(4):e108415.
10. Zhang H, Liesveld JL, Calvi LM, et al. The roles of bone remodeling in normal hematopoiesis and age-related hematological malignancies. *Bone Res*. 2023;11(1):15.
11. Landspersky T, Sacma M, Riviere J, et al. Autophagy in mesenchymal progenitors protects mice against bone marrow failure after severe intermittent stress. *Blood*. 2022;139(5):690-703.
12. Lopez-Otin C, Blasco MA, Partridge L, Serrano M, Kroemer G. Hallmarks of aging: an expanding universe. *Cell*. 2023;186(2):243-278.
13. Ma Y, Qi M, An Y, et al. Autophagy controls mesenchymal stem cell properties and senescence during bone aging. *Aging Cell*. 2018;17(1):e12709.
14. Gatica D, Lahiri V, Klionsky DJ. Cargo recognition and degradation by selective autophagy. *Nat Cell Biol*. 2018;20(3):233-242.
15. Liu ZZ, Hong CG, Hu WB, et al. Autophagy receptor OPTN (optineurin) regulates mesenchymal stem cell fate and bone-fat balance during aging by clearing FABP3. *Autophagy*. 2021;17(10):2766-2782.
16. Colom Díaz PA, Mistry JJ, Trowbridge JJ. Hematopoietic stem cell aging and leukemia transformation. *Blood*. 2023;142(6):533-542.
17. Zhu H, Guo ZK, Jiang XX, et al. A protocol for isolation and culture of mesenchymal stem cells from mouse compact bone. *Nat Protoc*. 2010;5(3):550-560.
18. Nakamura Y, Arai F, Iwasaki H, et al. Isolation and characterization of endosteal niche cell populations that regulate hematopoietic stem cells. *Blood*. 2010;116(9):1422-1432.
19. Weickert MT, Hecker JS, Buck MC, et al. Bone marrow stromal cells from MDS and AML patients show increased adipogenic potential with reduced Delta-like-1 expression. *Sci Rep*. 2021;11(1):5944.
20. Rachner TD, Link-Rachner CS, Bornhauser M, Hofbauer LC. Skeletal health in patients following allogeneic hematopoietic cell transplantation. *Bone*. 2022;158:115684.

21. Bartova E, Legartova S, Dundr M, Suchankova J. A role of the 53BP1 protein in genome protection: structural and functional characteristics of 53BP1-dependent DNA repair. *Aging (Albany NY)*. 2019;11(8):2488-2511.
22. Olivieri F, Albertini MC, Orciani M, et al. DNA damage response (DDR) and senescence: shuttled inflamma-miRNAs on the stage of inflamm-aging. *Oncotarget*. 2015;6(34):35509-35521.
23. Kruppa AJ, Kishi-Itakura C, Masters TA, et al. Myosin VI-dependent actin cages encapsulate parkin-positive damaged mitochondria. *Dev Cell*. 2018;44(4):484-499499.e6e486.
24. Kruppa AJ, Buss F. Actin cages isolate damaged mitochondria during mitophagy. *Autophagy*. 2018;14(9):1644-1645.
25. Florian MC, Dorr K, Niebel A, et al. Cdc42 activity regulates hematopoietic stem cell aging and rejuvenation. *Cell Stem Cell*. 2012;10(5):520-530.
26. Nalapareddy K, Zheng Y, Geiger H. Aging of intestinal stem cells. *Stem Cell Rep*. 2022;17(4):734-740.
27. Tiwari RL, Mishra P, Martin N, et al. A Wnt5a-Cdc42 axis controls aging and rejuvenation of hair-follicle stem cells. *Aging (Albany NY)*. 2021;13(4):4778-4793.
28. Gomes LC, Di Benedetto G, Scorrano L. During autophagy mitochondria elongate, are spared from degradation and sustain cell viability. *Nat Cell Biol*. 2011;13(5):589-598.
29. Konig T, Nolte H, Aaltonen MJ, et al. MIROs and DRP1 drive mitochondrial-derived vesicle biogenesis and promote quality control. *Nat Cell Biol*. 2021;23(12):1271-1286.
30. de Jonge JJ, Batters C, O'Loughlin T, Arden SD, Buss F. The MYO6 interactome: selective motor-cargo complexes for diverse cellular processes. *FEBS Lett*. 2019;593(13):1494-1507.
31. Tumbarello DA, Waxse BJ, Arden SD, Bright NA, Kendrick-Jones J, Buss F. Autophagy receptors link myosin VI to autophagosomes to mediate Tom1-dependent autophagosome maturation and fusion with the lysosome. *Nat Cell Biol*. 2012;14(10):1024-1035.
32. Ho TT, Warr MR, Adelman ER, et al. Autophagy maintains the metabolism and function of young and old stem cells. *Nature*. 2017;543(7644):205-210.
33. Harada K, Yahata T, Onizuka M, et al. Mitochondrial electron transport chain complex II dysfunction causes premature aging of hematopoietic stem cells. *Stem Cell*. 2023;41(1):39-49.
34. Wan MC, Tang XY, Li J, et al. Upregulation of mitochondrial dynamics is responsible for osteogenic differentiation of mesenchymal stem cells cultured on self-mineralized collagen membranes. *Acta Biomater*. 2021;136:137-146.
35. Li Q, Gao Z, Chen Y, Guan MX. The role of mitochondria in osteogenic, adipogenic and chondrogenic differentiation of mesenchymal stem cells. *Protein Cell*. 2017;8(6):439-445.
36. Zhang C, Li H, Li J, Hu J, Yang K, Tao L. Oxidative stress: a common pathological state in a high-risk population for osteoporosis. *Biomed Pharmacother*. 2023;163:114834.
37. Schreck C, Istvanffy R, Ziegenhain C, et al. Niche WNT5A regulates the actin cytoskeleton during regeneration of hematopoietic stem cells. *J Exp Med*. 2017;214(1):165-181.
38. Safiulina D, Kuum M, Choubey V, Hickey MA, Kaasik A. Mitochondrial transport proteins RHOT1 and RHOT2 serve as docking sites for PRKN-mediated mitophagy. *Autophagy*. 2019;15(5):930-931.
39. Qiu Y, Wang J, Li H, et al. Emerging views of OPTN (optineurin) function in the autophagic process associated with disease. *Autophagy*. 2022;18(1):73-85.
40. Fung TS, Chakrabarti R, Kollasser J, et al. Parallel kinase pathways stimulate actin polymerization at depolarized mitochondria. *Curr Biol*. 2022;32(7):1577-1592.e8.
41. Quach JM, Askmyr M, Jovic T, et al. Myelosuppressive therapies significantly increase pro-inflammatory cytokines and directly cause bone loss. *J Bone Miner Res*. 2015;30(5):886-897.
42. Weilbaecher KN. Mechanisms of osteoporosis after hematopoietic cell transplantation. *Biol Blood Marrow Transplant*. 2000;6(2A):165-174.
43. D'Souza AB, Grigg AP, Szer J, Ebeling PR. Zoledronic acid prevents bone loss after allogeneic haemopoietic stem cell transplantation. *Intern Med J*. 2006;36(9):600-603.
44. Russell RG. Bisphosphonates: mode of action and pharmacology. *Pediatrics*. 2007;119(suppl 2):S150-S162.
45. Dunford JE, Rogers MJ, Ebetino FH, Phipps RJ, Coxon FP. Inhibition of protein prenylation by bisphosphonates causes sustained activation of Rac, Cdc42, and Rho GTPases. *J Bone Miner Res*. 2006;21(5):684-694.
46. Tauchmanova L, Ricci P, Serio B, et al. Short-term zoledronic acid treatment increases bone mineral density and marrow clonogenic fibroblast progenitors after allogeneic stem cell transplantation. *J Clin Endocrinol Metab*. 2005;90(2):627-634.
47. Sweeney-Ambros AR, Biggs AE, Zimmerman ND, Mann KA, Damron TA, Oest ME. Orchestrated delivery of PTH [1-34] followed by zoledronic acid prevents radiotherapy-induced bone loss but does not abrogate marrow damage. *J Orthop Res*. 2022;40(12):2843-2855.
48. Lymperi S, Ersek A, Ferraro F, Dazzi F, Horwood NJ. Inhibition of osteoclast function reduces hematopoietic stem cell numbers in vivo. *Blood*. 2011;117(5):1540-1549.
49. Mansour A, Anginot A, Mancini SJ, et al. Osteoclast activity modulates B-cell development in the bone marrow. *Cell Res*. 2011;21(7):1102-1115.
50. Pundole X, Cheema HI, Petitto GS, Lopez-Olivo MA, Suarez-Almazor ME, Lu H. Prevention and treatment of bone loss and fractures in patients undergoing a hematopoietic stem cell transplant: a systematic review and meta-analysis. *Bone Marrow Transplant*. 2017;52(5):663-670.

51. Ebeling PR, Thomas DM, Erbas B, Hopper JL, Szer J, Grigg AP. Mechanisms of bone loss following allogeneic and autologous hemopoietic stem cell transplantation. *J Bone Miner Res*. 1999;14(3):342-350.

52. Serio B, Pezzullo L, Fontana R, et al. Accelerated bone mass senescence after hematopoietic stem cell transplantation. *Transl Med UniSa*. 2013;5(4):7-13.

53. Ukon Y, Makino T, Kodama J, et al. Molecular-based treatment strategies for osteoporosis: a literature review. *Int J Mol Sci*. 2019;20(10):2557.

54. Chandra A, Lagnado AB, Farr JN, et al. Targeted clearance of p21- but not p16-positive senescent cells prevents radiation-induced osteoporosis and increased marrow adiposity. *Aging Cell*. 2022;21(5):e13602.

55. Mukherjee S, Raje N, Schoonmaker JA, et al. Pharmacologic targeting of a stem/progenitor population in vivo is associated with enhanced bone regeneration in mice. *J Clin Invest*. 2008;118(2):491-504.

56. Chandra A, Wang L, Young T, et al. Proteasome inhibitor bortezomib is a novel therapeutic agent for focal radiation-induced osteoporosis. *FASEB J*. 2018;32(1):52-62.

57. Peterson JR, Lebensohn AM, Pelish HE, Kirschner MW. Biochemical suppression of small-molecule inhibitors: a strategy to identify inhibitor targets and signaling pathway components. *Chem Biol*. 2006;13(4):443-452.

58. Chandra A, Lin T, Young T, et al. Suppression of sclerostin alleviates radiation-induced bone loss by protecting bone-forming cells and their progenitors through distinct mechanisms. *J Bone Miner Res*. 2017;32(2):360-372.

59. Touaitahuata H, Blangy A, Vives V. Modulation of osteoclast differentiation and bone resorption by Rho GTPases. *Small GTPases*. 2014;5:e28119.

60. Yao S, Smiley SL, West K, et al. Accelerated bone mineral density loss occurs with similar incidence and severity, but with different risk factors, after autologous versus allogeneic hematopoietic cell transplantation. *Biol Blood Marrow Transplant*. 2010;16(8):1130-1137.